Galactic Diffuse Gamma-rays

M. Mori, Jan. 2001

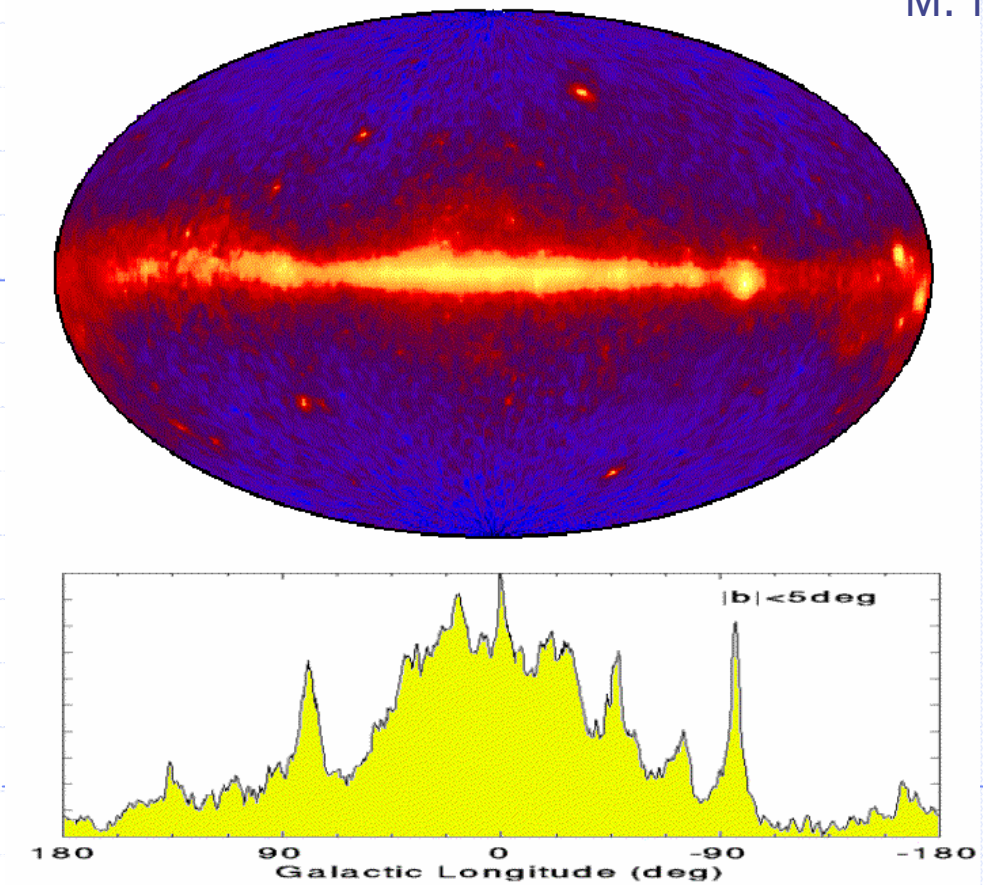

EGRET 100 MeV Sky

SAS-2 & COS-B Profile

SAS-2

(Thompson et al. 1976)

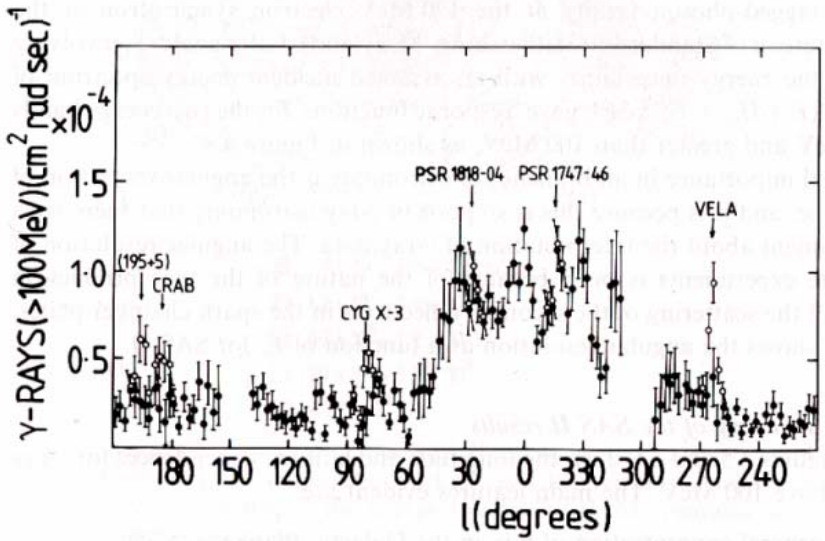

COS-B

(Mayer-Hasselwander et al. 1982)

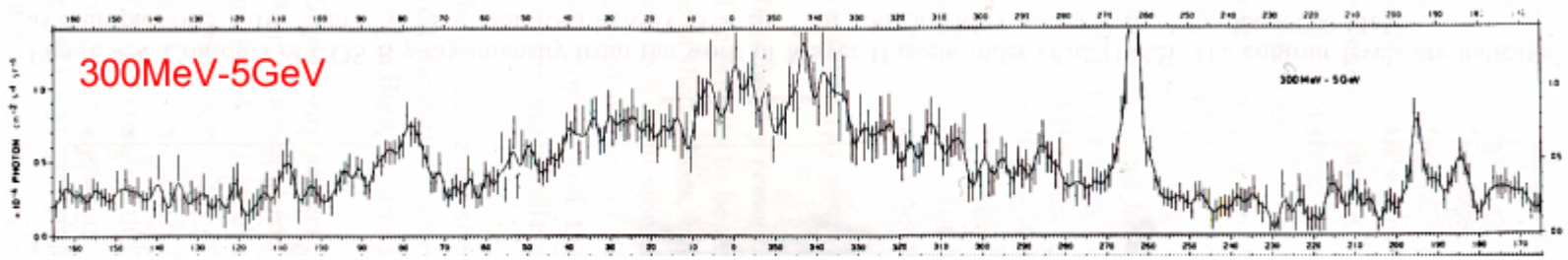

Figure 4.10. Longitude profiles of COS B γ-ray intensity averaged over $\pm 10°$ in latitude. Sold line: surface fitted to the data. (Mayer-Hasselwander *et al.* 1982.)

SAS-2 & COS-B Spectrum

Stecker 1979

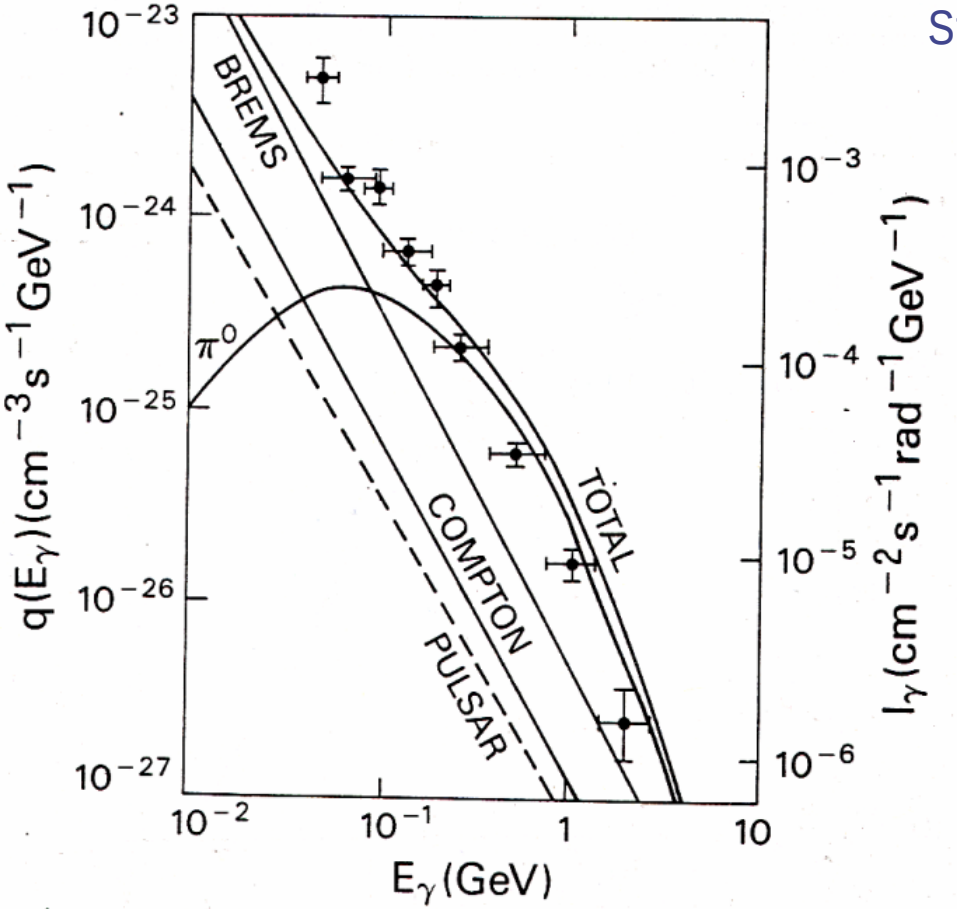

Fig. 4. Local differential production spectra for major diffuse production processes and the pulsar component as discussed in the text (left hand scale). The right hand scale and data points are from the COS-B and SAS-2 data in the longitude range around the galactic center and are shown in comparison to the predicted shape of the total spectrum.

EGRET Intensity Map

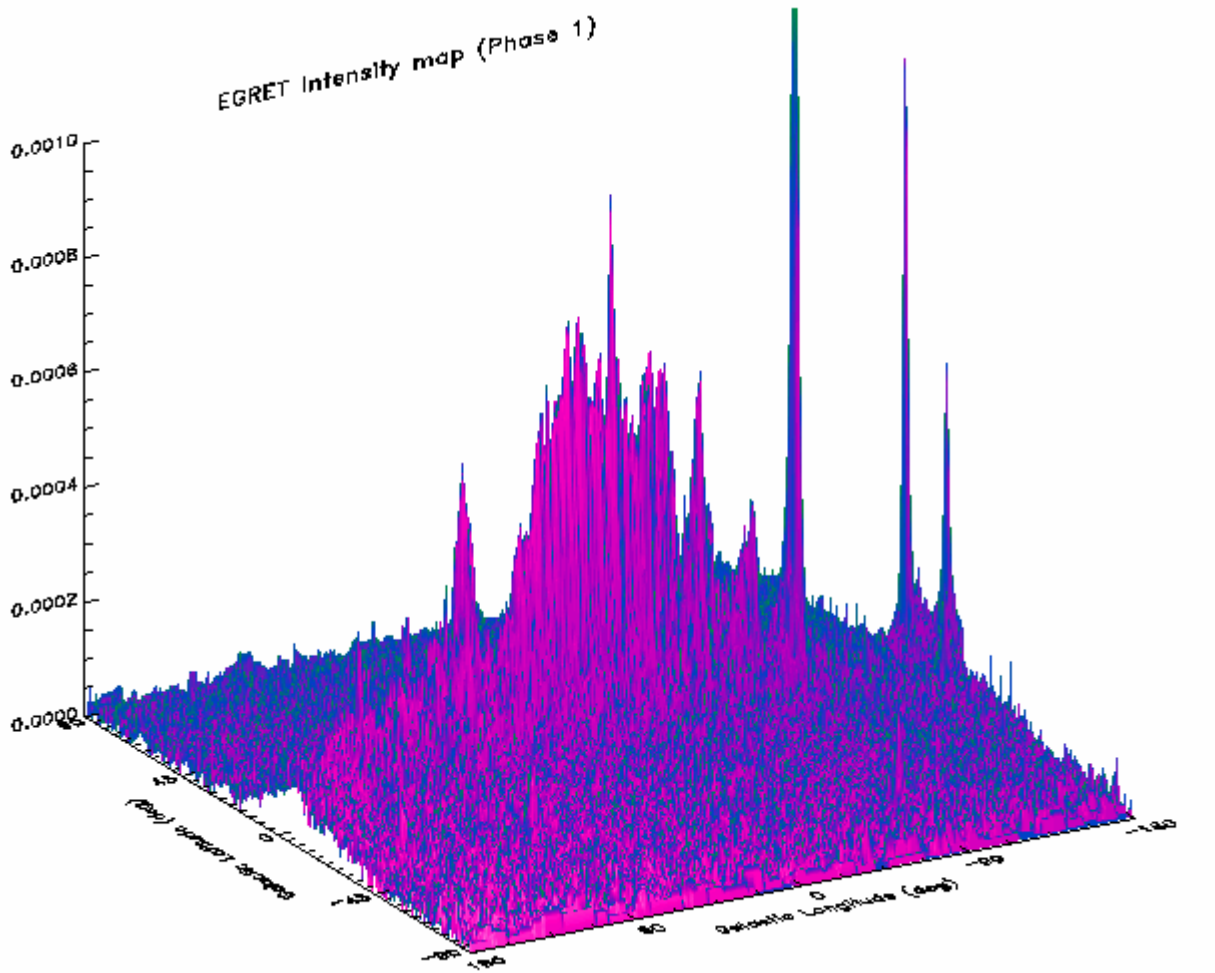

Diffuse Emission Model

- Three main components:
  - Bremsstrahlung: electron + matter $\rightarrow \gamma$ + X
  - Inverse Compton: electron + photons $\rightarrow \gamma$ + X
  - Nuclear interaction: proton(nuclei) + matter $\Rightarrow \pi^0 \rightarrow 2\gamma$

Matter = HI + HII + H_2
Photon = 2.7K BB + FIR + NIR + Optical + UV

Galactic Matter Distribution

- HI : 21cm surveys
  Weaver & Williams (1973)
  Maryland-Parkes (1986)
  Leiden-Green Bank (1985)

Bertsch et al. 1993

- H_2 : $N(H_2) = X\, W_{CO}$
  CO: Columbia CO survey at 2.6mm (1987)
- HII : Taylor & Cordes (1993)
  (pulsar dispersion / interstellar scattering measure)
- Interstellar radiation field : 2.7K BB + FIR + NIR + Optical + UV
- Local Electron spectrum : Skibo (1993) [$E^{-2.42}$ injection]
- Local Proton spectrum : Stecker (1970) [$E^{-2.7}$]
- Cosmic-ray enhancement factor $\rho \propto N(\mathrm{HI}) + N(H_2) + N(\mathrm{HII})$
  Gaussian along the Galactic axis (scaling parameter r_0)

Only two parameters in this model :

$X = (1.5 \pm 0.2) \times 10^{20}$ H-mol cm^{-2}(K km s^{-1})$^{-1}$

$r_0 = (2.0 \pm 0.5)$ kpc

Cosmic-ray Enhancement Factor

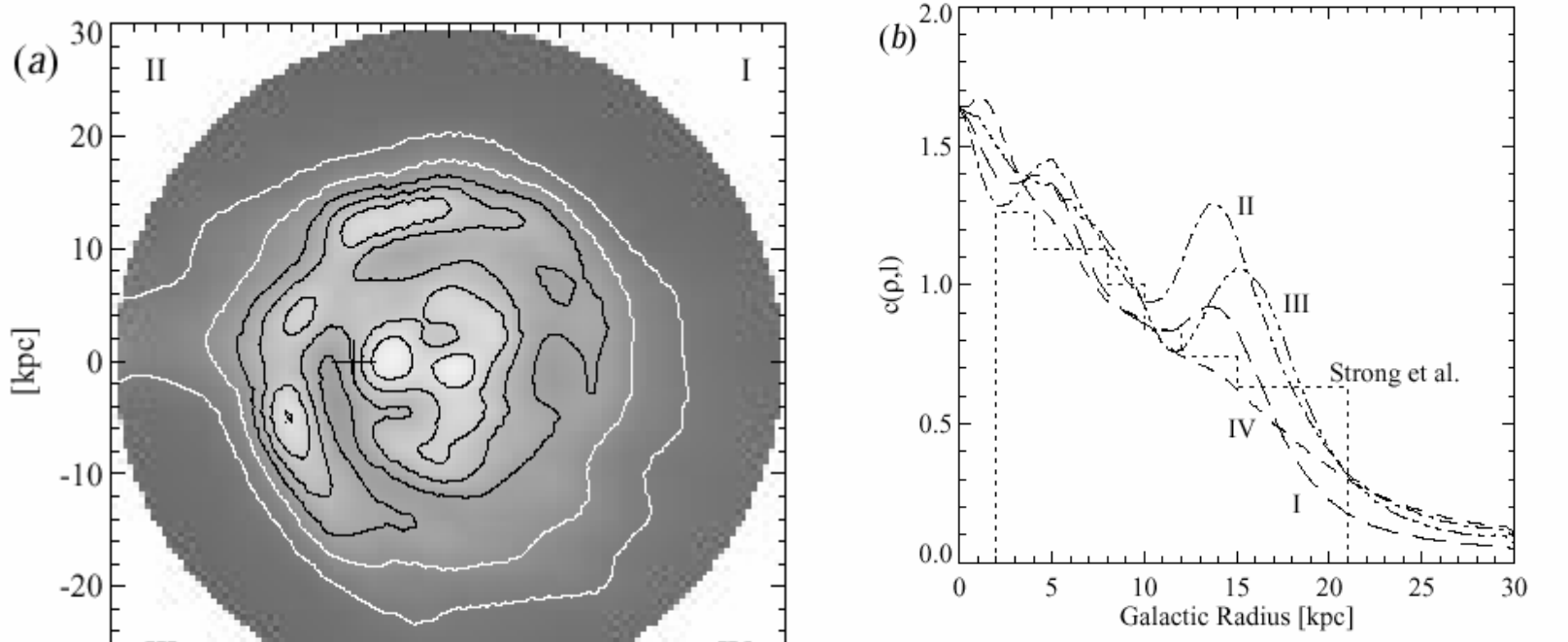

FIG. 9.—(*a*) The cosmic-ray enhancement factor $c(\rho, l)$ derived by convolving the sum of the H I, H_2, and H II surface densities from Fig. 8 with a Gaussian with FWHM equal to the best-fit value of $r_0 = 1.76$ kpc (see § 5). The enhancement factor is normalized to unity at the position of the Sun, indicated by the cross. (*b*) The azimuthal average of the cosmic-ray enhancement factor for each Galactocentric quadrant indicated in (*a*). The azimuthally symmetric gamma-ray emissivity, which is proportional to the cosmic-ray enhancement factor, determined by Strong et al. (1988, 150–300 MeV, their case 3, scaled to $R_\odot = 8.5$ kpc, and normalized to unity in the 8–10 kpc ring) is indicated by the dotted line.

EGRET Diffuse Emission Model

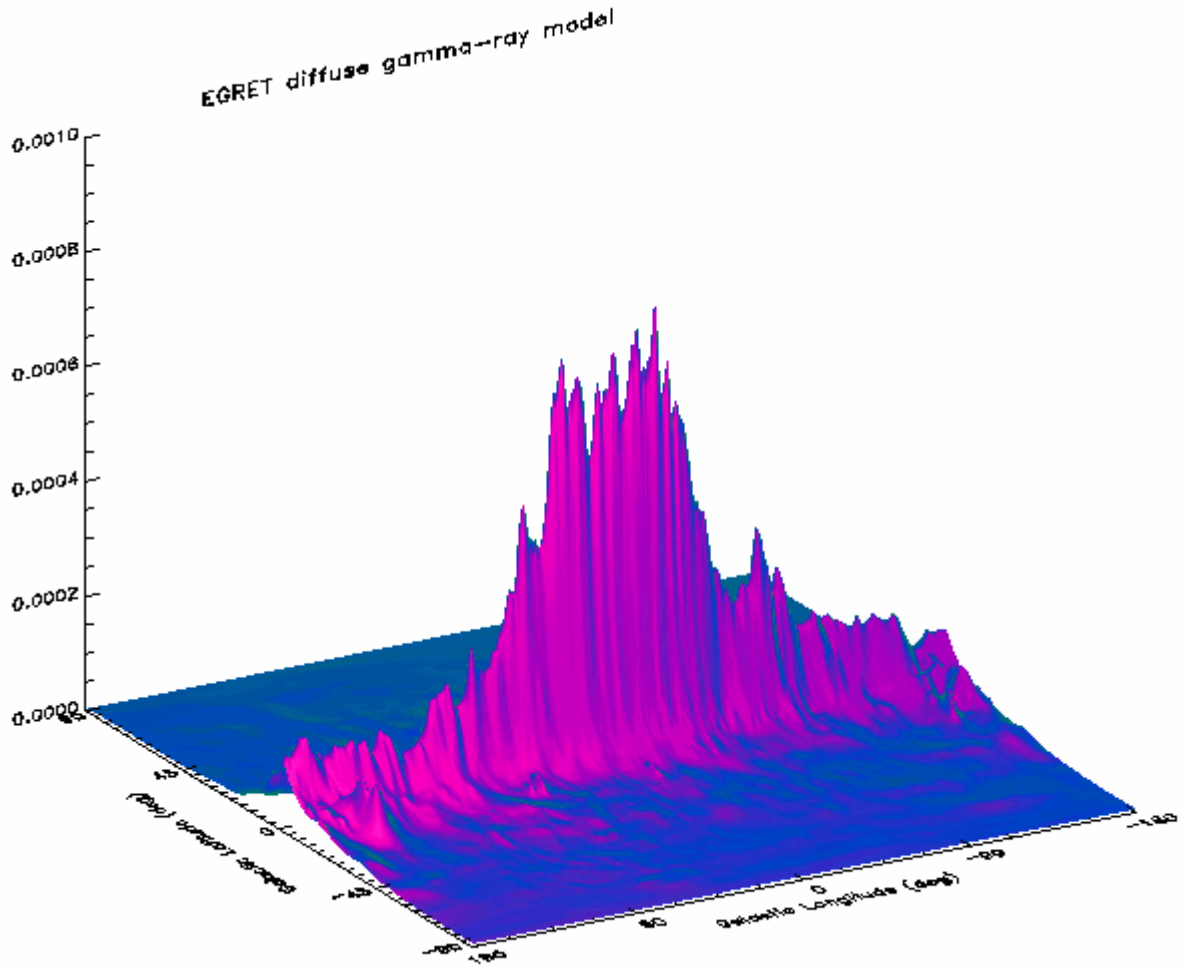

Sources = Observed – Model

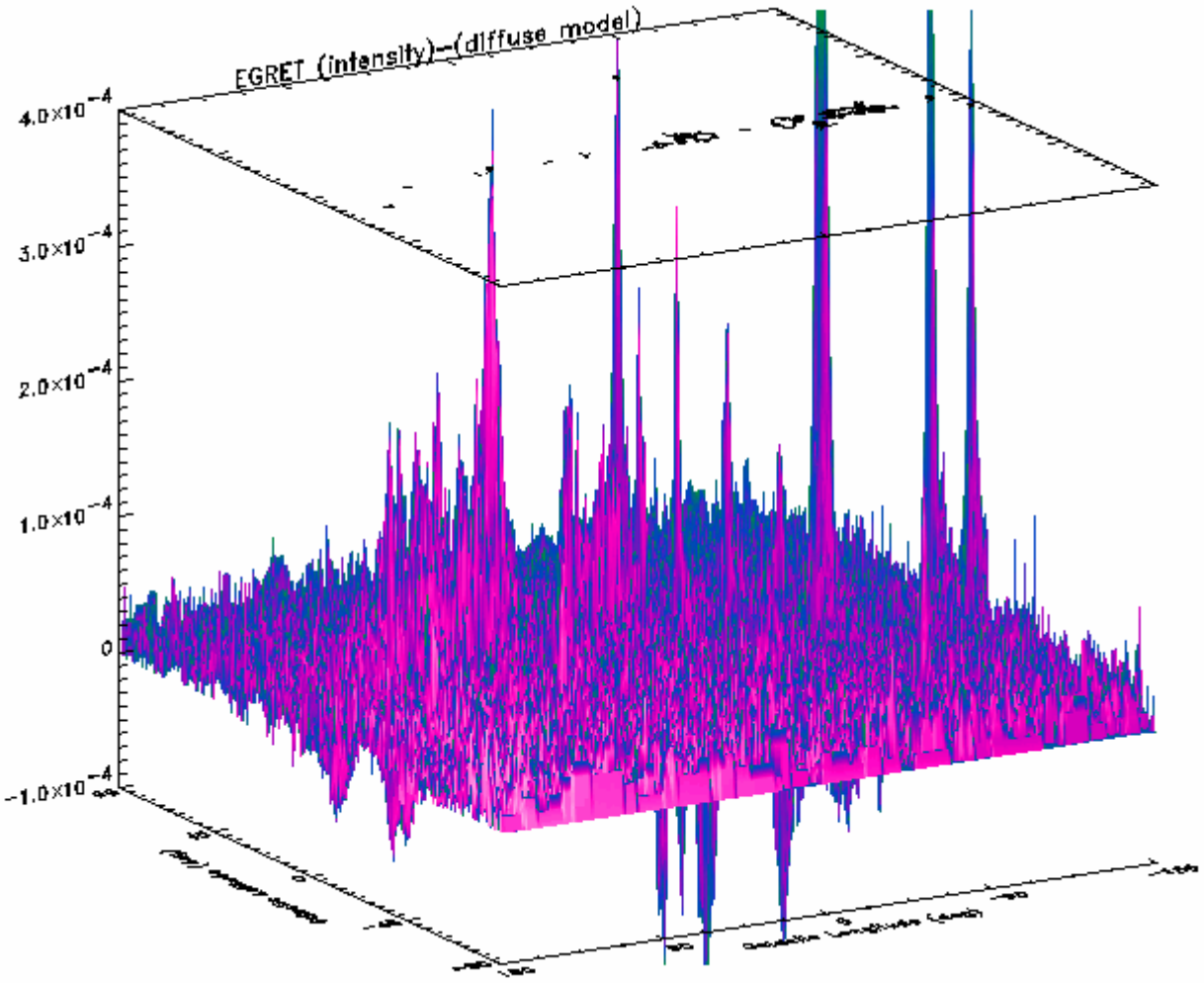

Longitudinal Profile

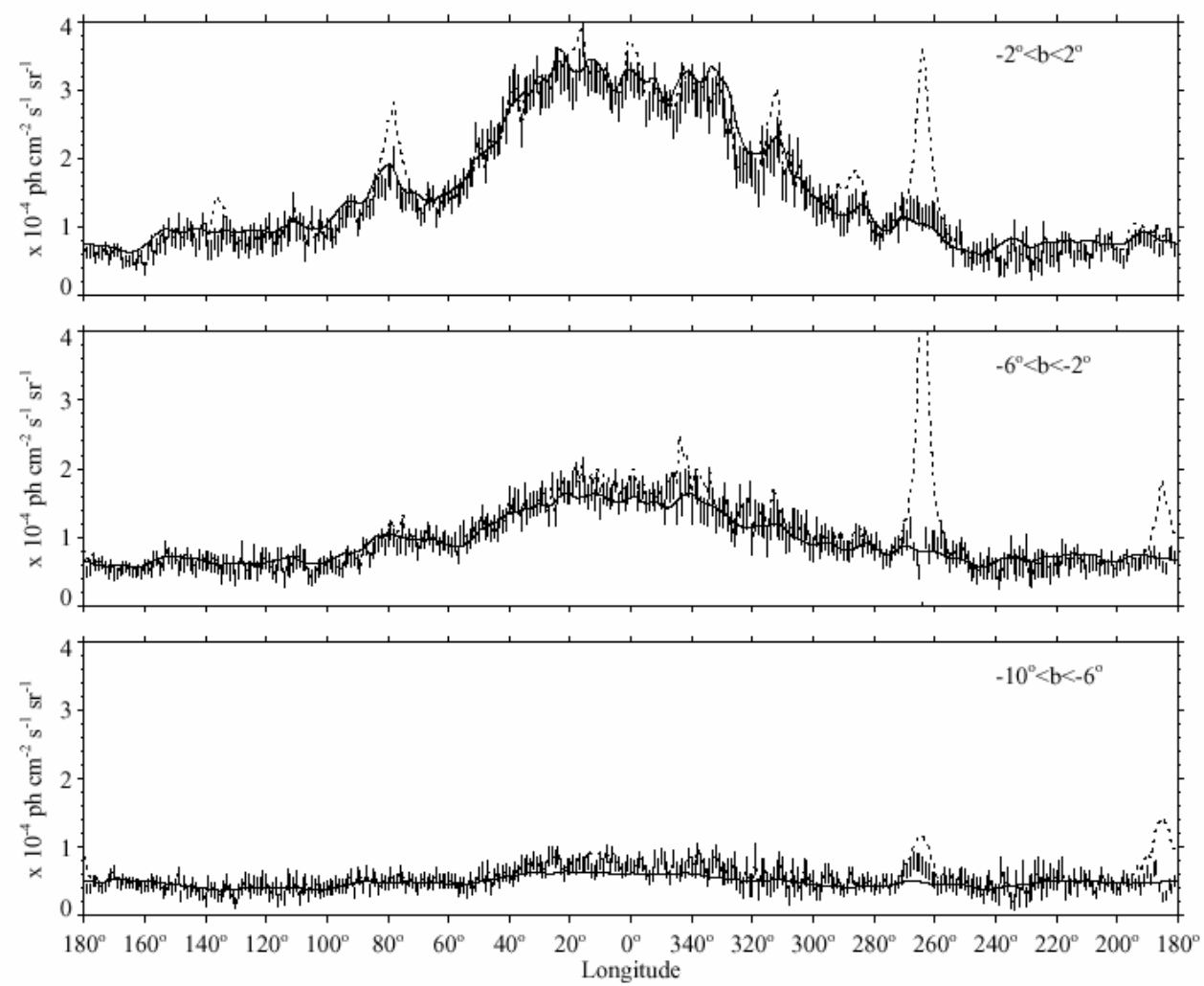

100-300 MeV

Latitude Profile

100-300 MeV

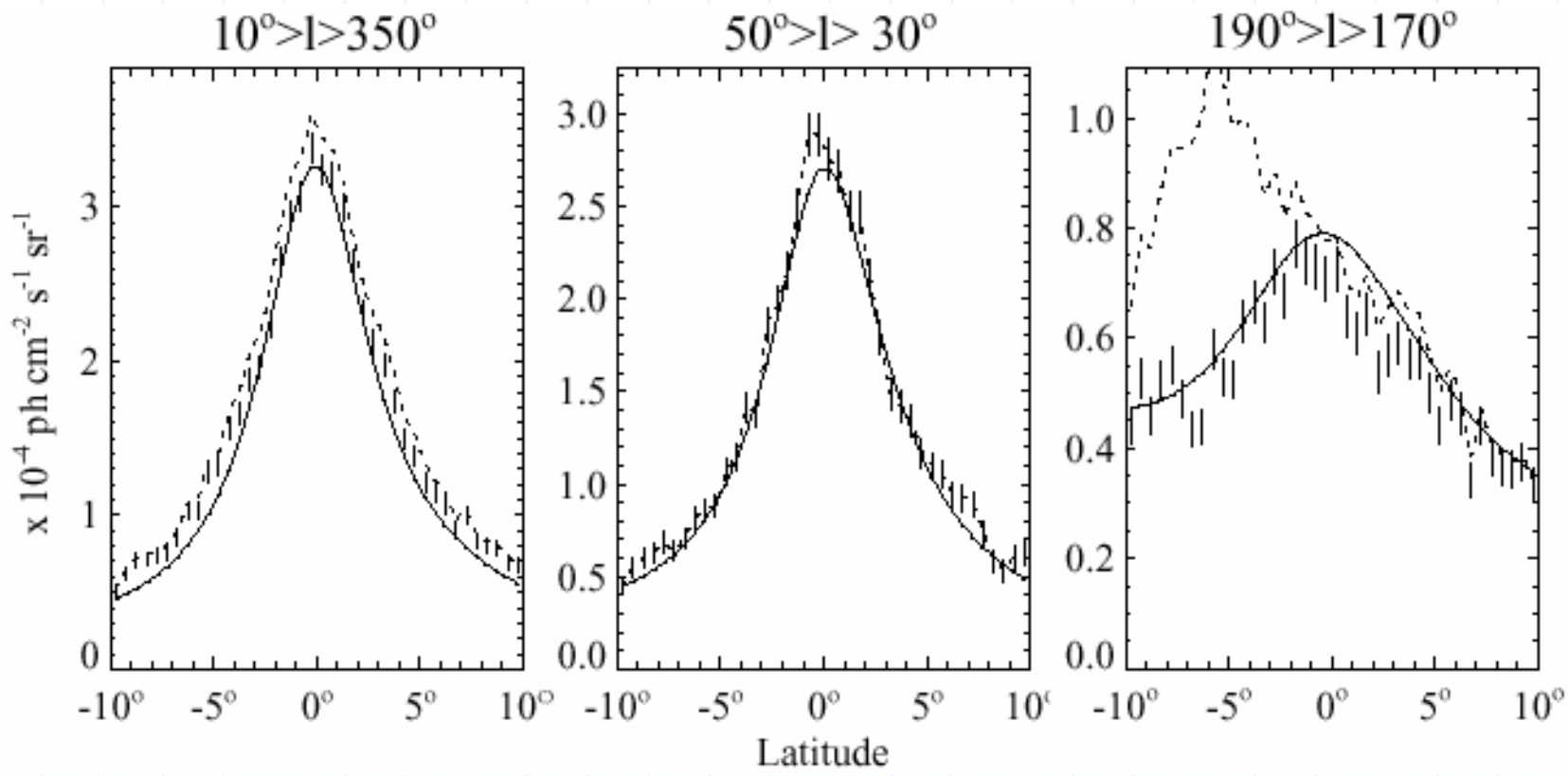

EGRET spectrum

- Hunter et al. 1997

FIG. 4.—Average diffuse gamma-ray spectrum of the inner Galaxy region, $300° < l < 60°$, $|b| \leq 10°$(0.73 sr). The contributions from point sources detected with more than 5 σ significance have been removed. The data are plotted as crosses where the horizontal line indicates the width of the energy interval and the vertical line the ± 1 σ statistical error. The intensity and error for the four lowest energy intervals include corrections to the EGRET effective area derived using observations of the Crab pulsar (Thompson et al. 1993b). The best-fit model calculation (see § 5) plus the isotropic diffuse emission is shown as the solid line. The individual components of this calculation, nucleon-nucleon (NN), electron bremsstrahlung (EB), and inverse Compton (IC), are shown as dashed lines. The isotropic diffuse emission (ID, Sreekumar et al. 1997) is shown as a dash-dotted line.

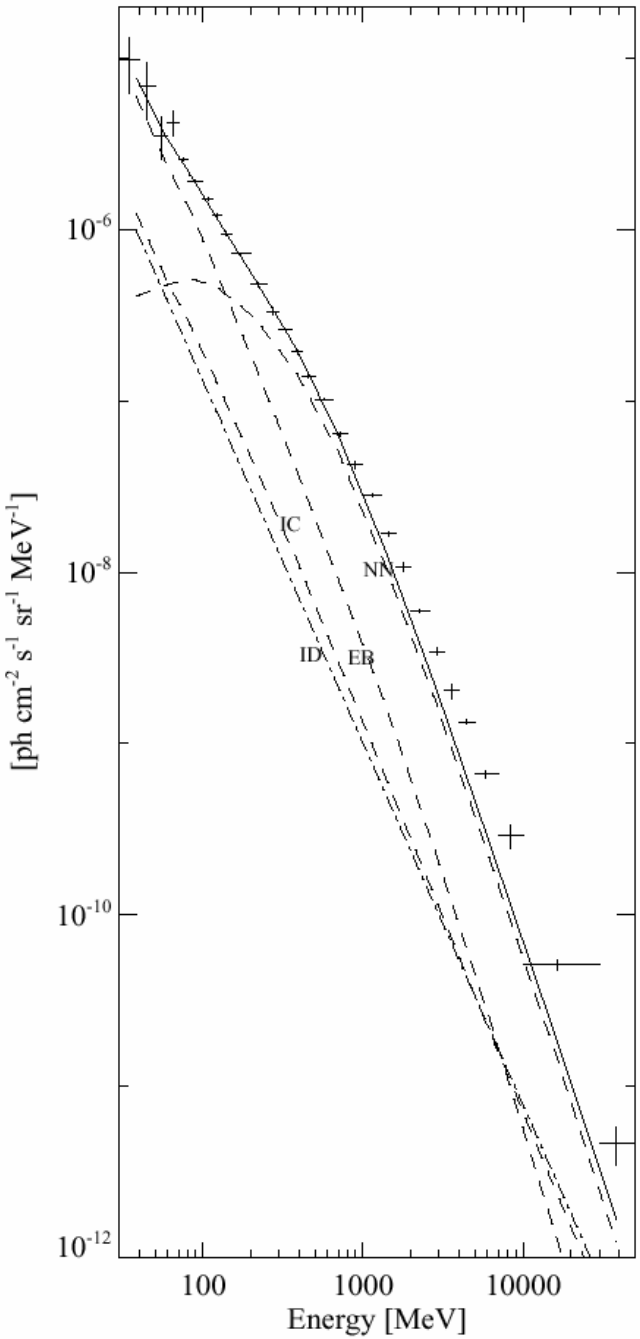

Observation by EGRET

○ $|b| \leq 10°$, 38 point sources ($>5\sigma$) removed

◎ 30MeV - 50GeV with excellent statistics (cf. COS B)

◎ General agreement with model predictions in spatial profile

● 40-60% excess against model predictions above 1 GeV

⇒ Possible solutions:

- Instrumental calibration error?
- Unresolved sources?
- Nuclear interaction model?
- Cosmic-ray spectrum?

Flatter Proton Spectrum? -1

Mori 1997

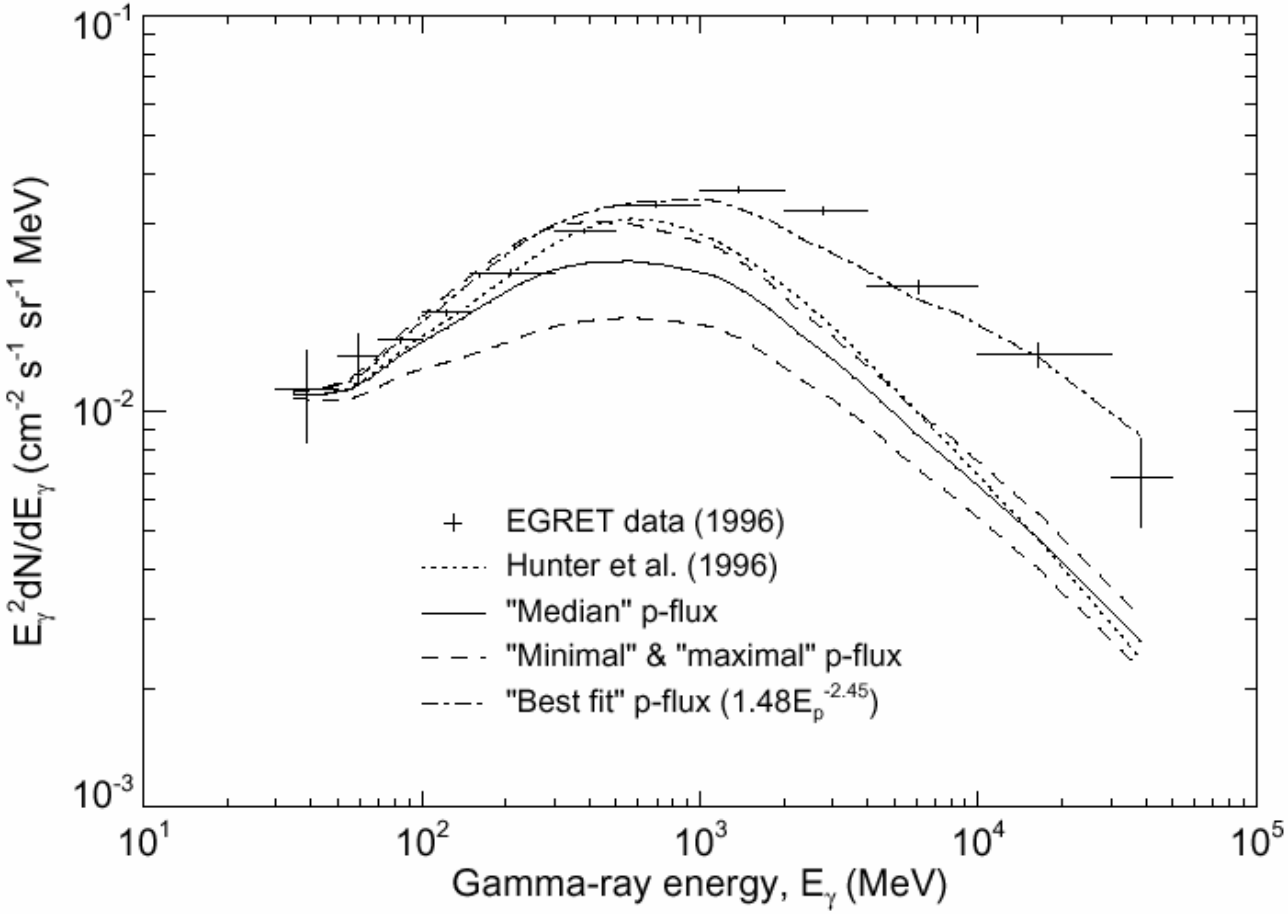

Standard:

$E^{-2.7}$

↓

$E^{-2.45}$?

Flatter Proton Spectrum? -2

Völk 2000

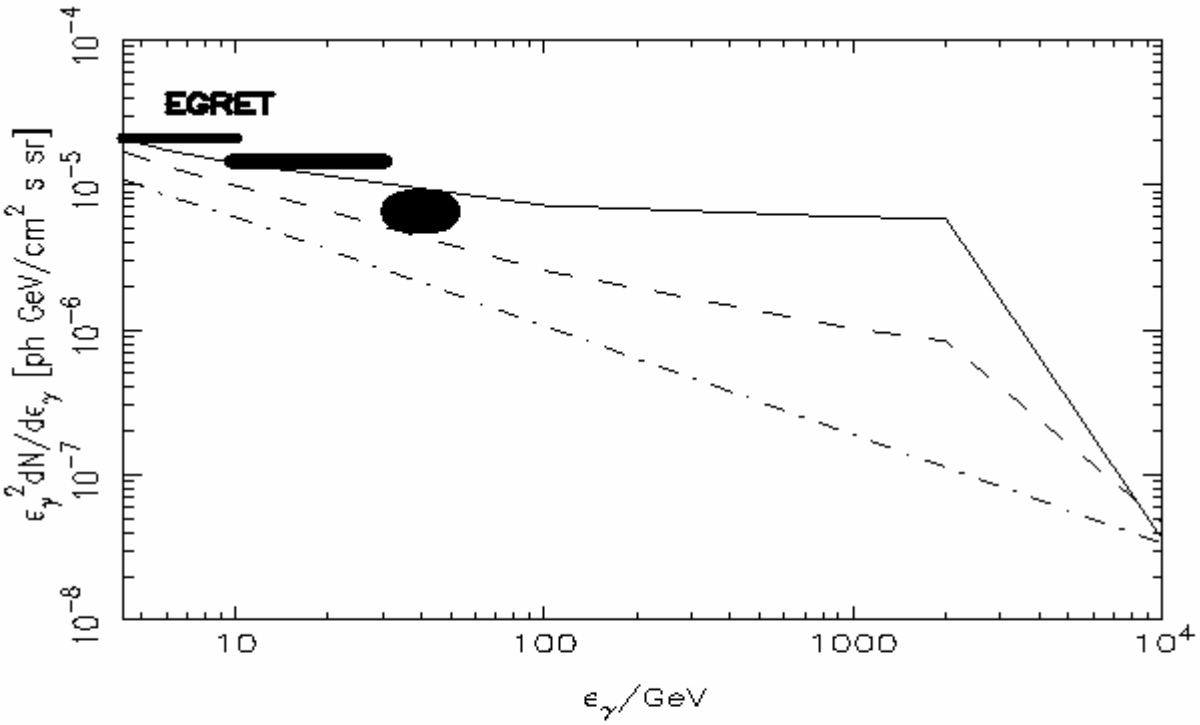

Souce: E^{-2}

↓

Transport effect

FIGURE 1. The differential diffuse γ-ray energy flux vs γ-ray energy above 4.4 GeV (cf. Berezhko & Völk, 1999). The heavy symbols are the EGRET measurements, and the dash-dot line is the model prediction of Hunter et al. (1997a). The full curve corresponds to our acceleration model with $\gamma_{SCR} = 2$, whereas the dashed curve corresponds to the Leaky Box model. Both theoretical curves incorporate energy-dependent loss from the acceleration region.

Flatter Inverse Compton? -1

Porter & Prothroe 1997

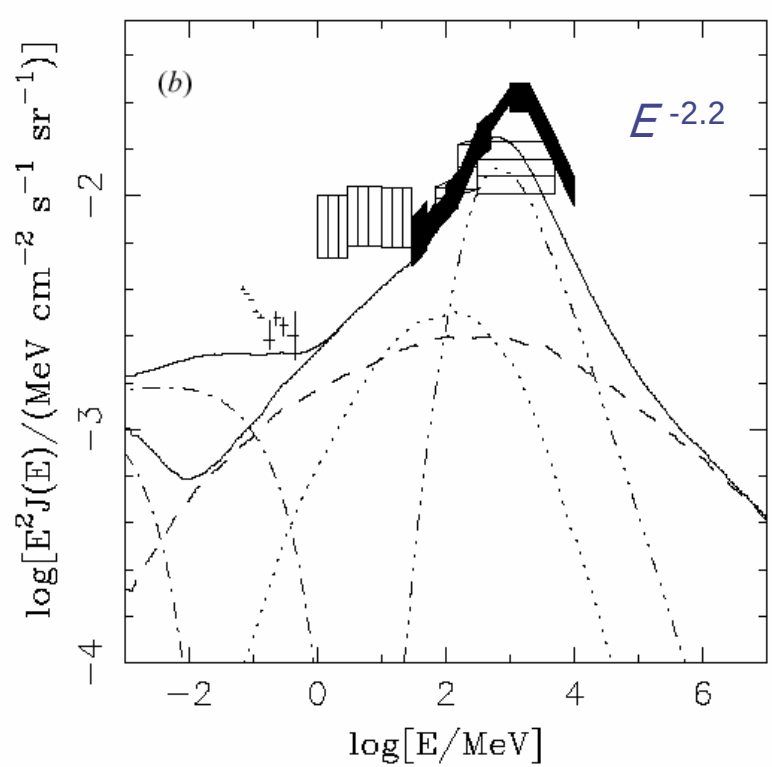

Figure 6. Average gamma-ray spectra for the inner Galaxy ($-60^\circ < l < 60^\circ$ and $|b| < 20^\circ$) for an injection spectrum of (*a*) $E^{-2.4}$ and (*b*) $E^{-2.2}$. The individual contributions to the diffuse gamma-ray spectrum are indicated: IC by the broken curve; bremsstrahlung by the dotted curve; synchrotron by the chain curve; π^0-decay by the double chain curve. The full curve is the sum of all contributions. Data are from various satellite telescopes; blocked data: EGRET [22], horizontally hatched boxes: COS-B [18], vertically hatched boxes: COMPTEL [12], and data points: OSSE [12] (original data from [20]).

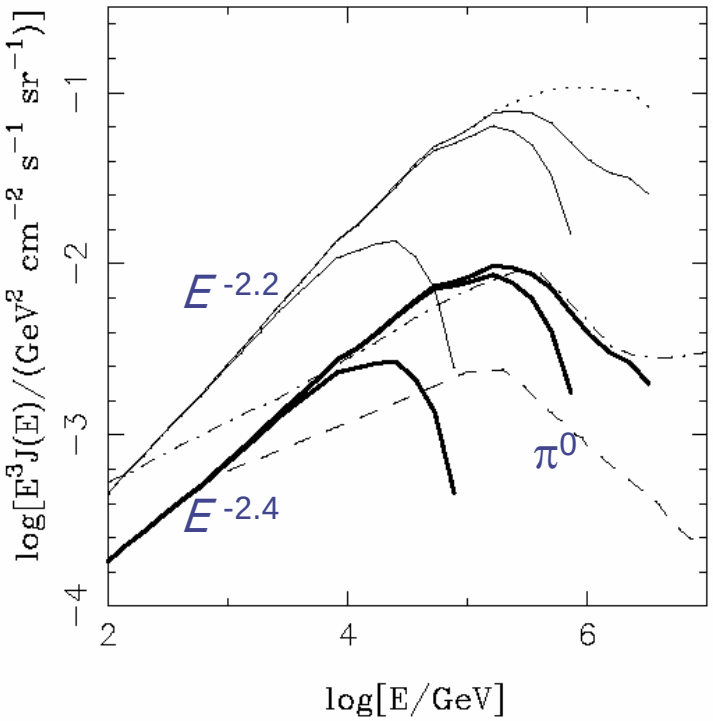

Figure 7. Diffuse gamma-ray spectra in the direction $l = 0^\circ$, $b = 0^\circ$. Heavy full curves show the IC spectrum for an $E^{-2.4}$ injection spectrum of electrons; light full curves show the IC spectrum for $E^{-2.2}$. For each injection spectrum, the lowest branch is for a cut-off at 100 TeV, the next higher branch a cut-off at 1 PeV, and the next higher no cut-off in the injection spectrum; each of these curves includes attenuation on the CMBR. The dotted curve shows the IC spectrum for an $E^{-2.2}$ spectrum with no cut-off and no attenuation on the CMBR. The chain curve shows the predicted spectrum for π^0-decay (including attenuation on the CMBR) calculated by Ingelman and Thunman [63]; the broken curve shows the predicted π^0-decay spectrum (including attenuation on the CMBR) calculated by Berezinsky *et al* [62].

Flatter Inverse Compton? -2

Pohl & Esposito 1998

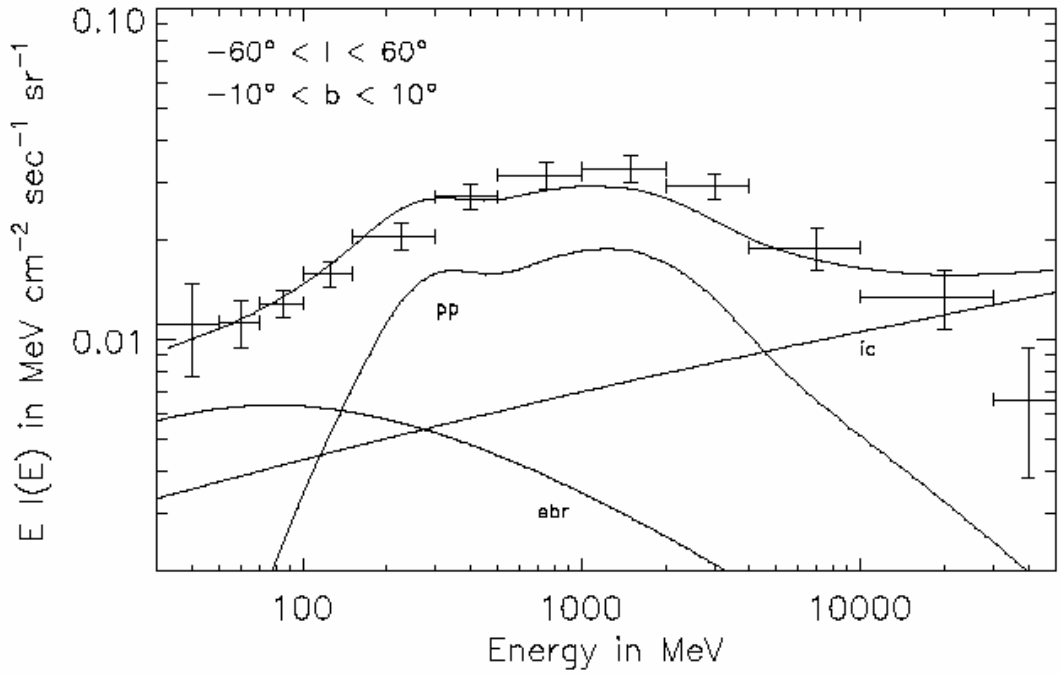

Distributed

$E^{-2.0\pm0.2}$

FIG. 5.—Gamma-ray intensity in the direction of the inner Galaxy. The data points are taken from Hunter et al. (1997). The error bars include an estimate for the systematic error of 8%, which accounts for the uncertainty in the energy-dependent correction of the spark chamber efficiency (Esposito et al. 1998). The data are compared with bremsstrahlung ("ebr") and Inverse Compton ("ic") spectra from our model, on the basis of sources with injection indexes following a normal distribution of mean 2.0 and dispersion 0.2 and the spatial distribution of SNRs in spiral arms. The π^0-component is a template and not a model.

Contribution of each components

Hunter et al. 1997

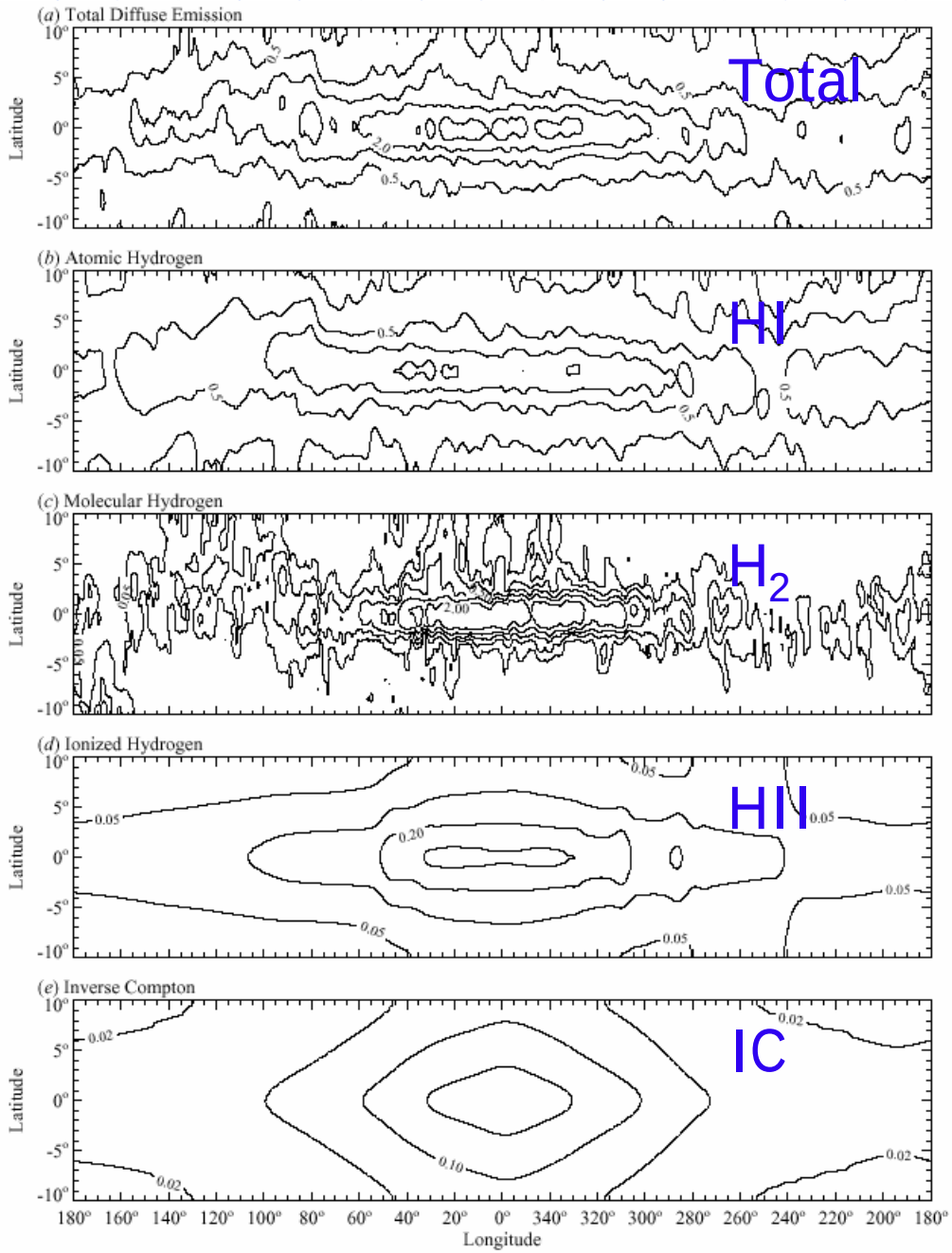

Higher energy? Amenomori et al. 1997

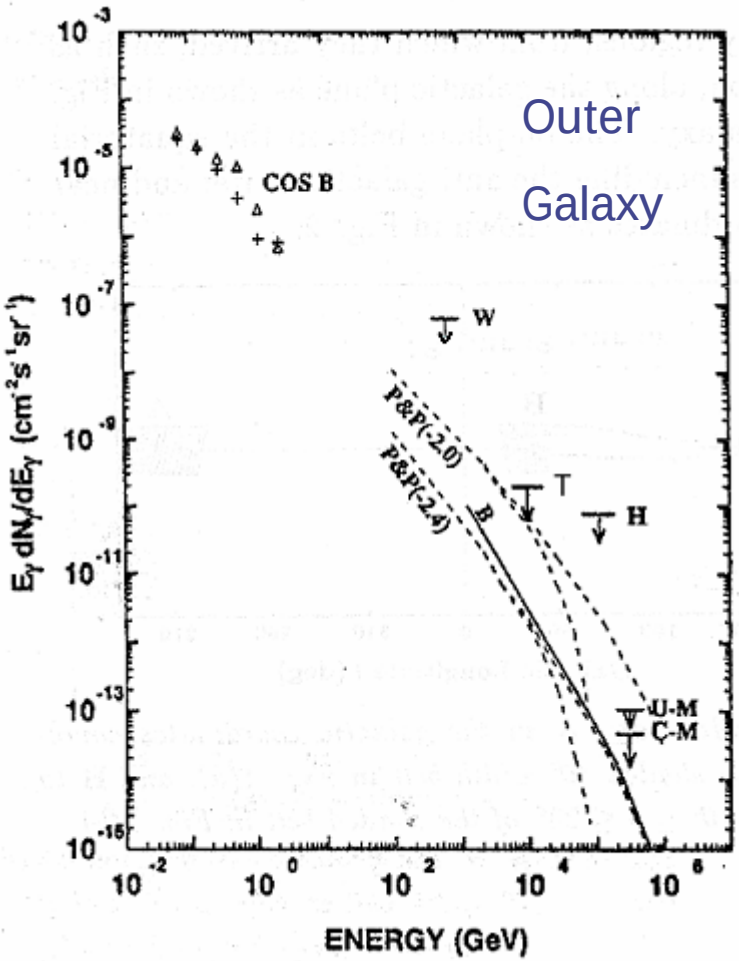

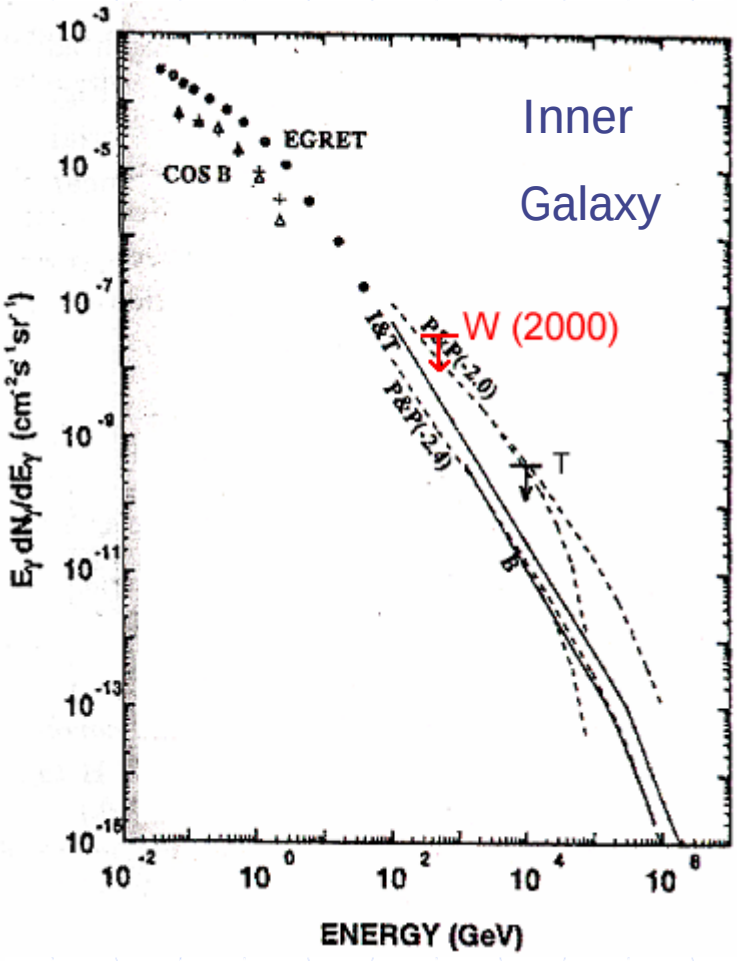

Fig. 4 Diffuse gamma rays from the outer Galaxy. The plotted points are **COS-B** *data (Paul et al. 1978); (△): 91° ≤ l ≤ 110°, | b |≤ 10°; (+): 116° ≤ l ≤ 136°, b |≤ 10°. Present data (***Tibet***) is given by the upper limit at 10 TeV for 140° ≤ l ≤ 225°, | b |≤ 5°. The ground based data are shown by* **U-M** *(Utah-Michigan, Matthews et al. 1991) for 30° ≤ l ≤ 220°, | b |≤ 10° and* **C-M** *(CASA-MIA, Borione et al. 1991) for 50° ≤ l ≤ 200°, | b |≤ 10°. The other upper limits assigned by* **W** *(Whipple, Reynolds et al. 1993) and* **H** *(HEGRA, Karle et al. 1995) are data for wide sky regions apart from the galactic disk. The theoretical curves are assigned by* **B** *(Berezinsky et al. 1993) for $\pi^0 \rightarrow 2\gamma$ decay and* **P&P** *(Porter & Protheroe 1996) for the inverse Compton by electrons with injected spectral indeces -2.0 and -2.4, respectively. Lower curves of* **P&P** *are the case of energy cut at 100 TeV for the shock acceleration.*

Fig. 5 Diffuse gamma rays from the inner Galaxy. The plotted points are **COS-B** *data (Paul et al. 1978); (△): 16° ≤ l ≤ 36°, | b |≤ 10°; (+): 315° ≤ l ≤ 36°, | b |≤ 10°, and* **EGRET** *data (Hunter et al. 1997); (●): 300° ≤ l ≤ 60°, | b |≤ 10°. Present data (***Tibet***) is given by the upper limit at 10 TeV for 20° ≤ l ≤ 55°, | b |≤ 5°. In addition to the theoretical curves* **B** *and* **P&P** *in Fig. 4,* **I&T** *(Ingelman & Thunman 1996) for $\pi^0 \rightarrow 2\gamma$ decay is shown by a dot-dot-dashed curve.*

Air Shower Observations

- CASA-MIA (Borione et al. 1998)
  $50^\circ < l < 200^\circ$, $-5^\circ < b < 5^\circ$; 310 TeV
  mu-poor showers $\Rightarrow I_\gamma / I_{CR} < 2.4 \times 10^{-5}$
- Tibet (Amenomori et al. 1997)
  $-5^\circ < b < 5^\circ$, 10 TeV, excess counts $\Rightarrow$
  $140^\circ < l < 225^\circ$: $< 2 \times 10^{-10}$ cm^{-2}s^{-1}sr^{-1}
  $20^\circ < l < 55^\circ$: $< 4 \times 10^{-10}$ cm^{-2}s^{-1}sr^{-1}
- EAS-TOP (Aglietta et al. 1996); 1 PeV
  mu-poor showers $\Rightarrow I_\gamma / I_{CR} < 7.3 \times 10^{-5}$
- HEGRA (Karle et al. 1995); 80 TeV
  N_e/Ch cut $\Rightarrow I_\gamma / I_{CR} < 7.8 \times 10^{-3}$

Whipple observation

LeBohec et al. 2000

- 4.8° FOV camera, Center: (l,b)=(40,0)
- 1998: 7 on/off pairs (28min. Each), >700GeV
  1999: 10 on/off pairs, >500GeV
- Sensitivity correction across the field

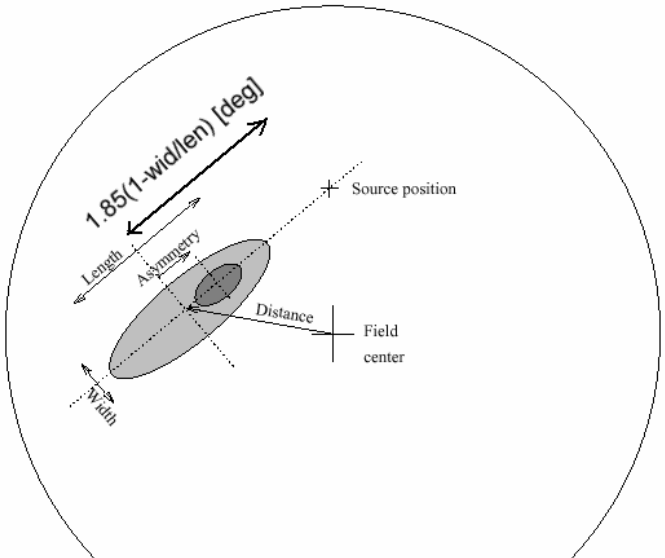

GAMMA-RAY CANDIDATE SELECTION

Parameters	Selection Criteria
Max1 (d.c.)	>78
Max2 (d.c.)	>56
Width (deg)	$0.073 < w < 0.16$
Length (deg)	$0.16 < l < 0.43$
Distance (deg).....	$d < 1.8$

NOTE.—d.c. = digital counts; 1 d.c. ≃ 1 photoelectron.

Whipple results

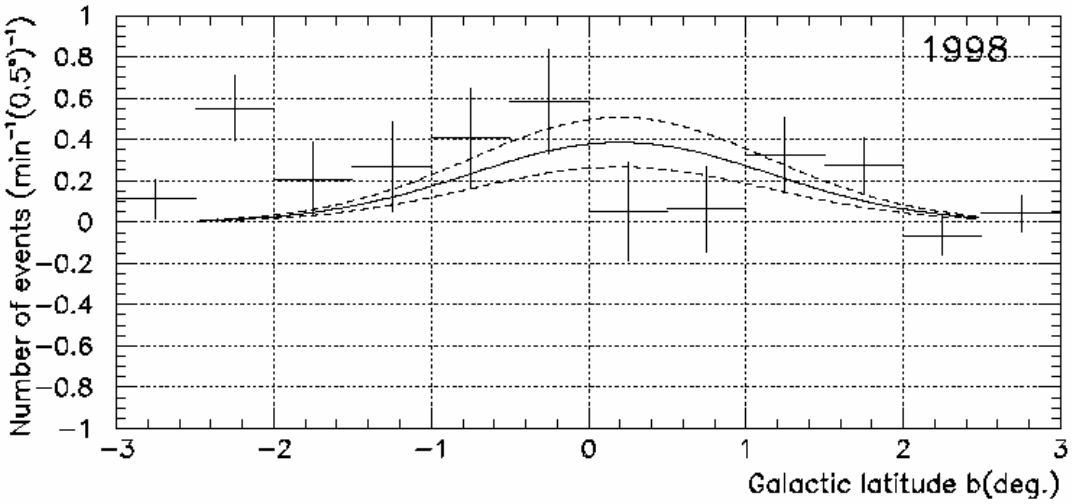

Fig. 6*a*

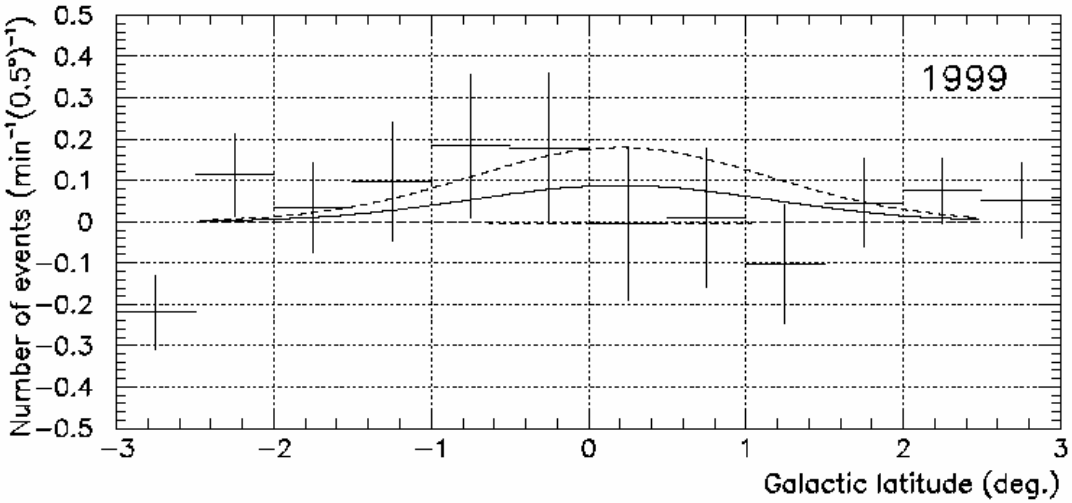

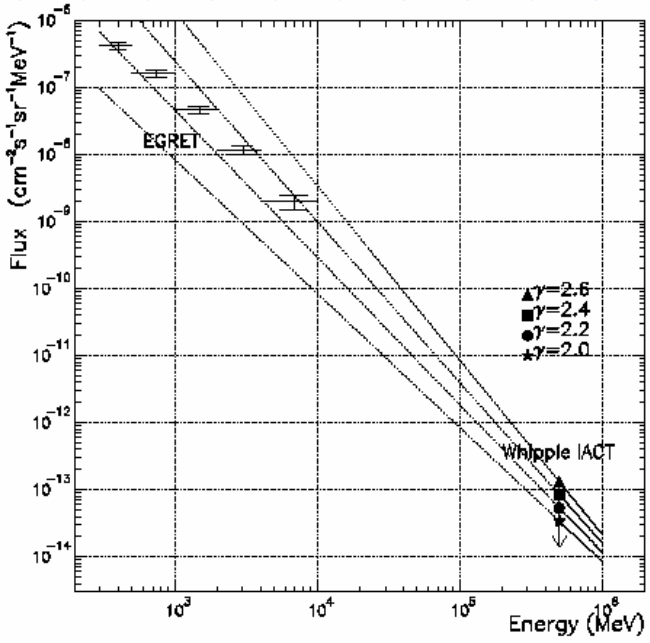

1998: 1.84±0.57/min (3.2σ!)

1999: 0.42±0.43/min

HEGRA observations

Pühlhofer et al. 1999

Lampeitl et al. 1999

- 4-telescope setup, total 105hr (1997/98)
- No source candidate above ¼ Crab
- Artificial Neural Network analysis for gamma/hadron separation in progress

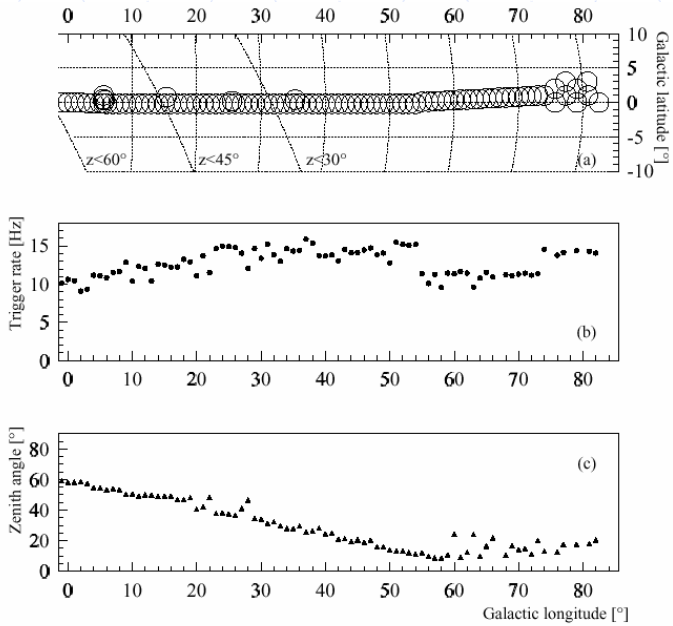

Figure 1: (a) Observed regions in Galactic coordinates. The circles indicate the field of view of the telescope system. The diagonal lines mark culmination zenith angles (from left to right) 60°, 45° and 30°. (b) Mean trigger rates. (c) Zenith angles of the observations.

Limits from Balloon Experiments

Hunter 2000

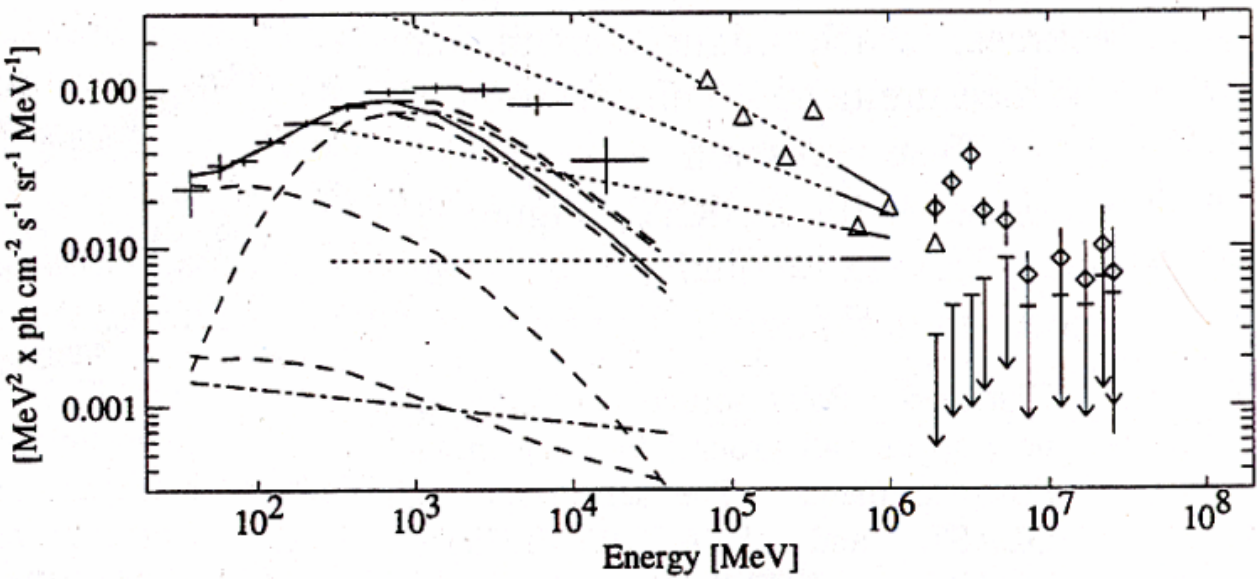

Figure 8. Measurement of the Galactic diffuse emission > 50 GeV with the Whipple telescope [29] extrapolated to the EGRET energy range on the assumption of single power-law spectral indices of 2.0, 2.2, 2.4, and 2.6. The spectral index must be ⩽2.4 to be consistent with the EGRET observations, shown as ±1 σ data points. The unpointed balloon results from Nishimura et al. [28] and the JACEE experiment [27], taken at 4 gm/cm^2 and 5.5 gm/cm^2, shown as triangles and diamonds, respectively, should be treated as upper limits. The JACEE results corrected for the atmospheric contribution are shown as upper limits.

Summary

- Diffuse gamma-rays above 1 GeV shows a flatter spectrum than expected
- Observation of the Galactic Plane, especially near the Galactic Center is scarce in the TeV region
- Imaging can increase sensitivity
- *Do it with CANGAROO!*

CANGAROO schedule